

## Sea-Ice Floes Identification and Detection using Matlab

**T. Ravichandra Babu****Associate Professor & HOD,****Department of ECE,****Krishnamurthy Institute of Technology and  
Engineering.****Eman Bhattacharjee****PG Scholar-SSP,****Department of ECE,****Krishnamurthy Institute of Technology and  
Engineering.**

### Abstract:

An unmanned aerial vehicle was used as a mobile sensor platform to collect sea-ice features at Ny-Ålesund in early May 2011, and several image processing algorithms have been applied to samples of sea-ice images to extract useful information about sea ice. The sea-ice statistics given by the floe size distribution, being an important parameter for climate and wave- and structure-ice analysis, is challenging to calculate due to difficulties in ice floe identification, particularly the separation of seemingly connected ice floes. In this paper, the gradient vector flow (GVF) snake algorithm is applied to solve this problem. To evolve the GVF snake algorithm automatically, an initialization based on the distance transform is proposed to detect individual ice floes, and the morphological cleaning is afterward applied to smoothen the shape of each identified ice floe. Based on the identification result, the image is separated into four different layers: ice floes, brash pieces, slush, and water. This makes it further possible to present a color map of the ice floes and brash pieces based on sizes, and the corresponding ice floe size distribution histogram. The proposed algorithm yields an acceptable identification result, and its effectiveness is demonstrated in a case study. A discussion on the methods and results concludes the paper.

### I. INTRODUCTION:

SEA ICE, which is defined as any form of ice that forms as a result of seawater freezing [1], covers

approximately 7% of the total area of the world's oceans [2]. It is turbulent because of wind, wave, and temperature fluctuations. Various types of sea ice can be found in ice-covered regions. Ice floe, which is the flat pieces of sea ice, can range from meters to kilometers in size. The floe size distribution is a basic parameter of sea ice that affects the behavior of sea-ice extent, both dynamically and thermodynamically. Particularly for relatively small ice floes, it is critical to the estimation of melting rate [3]. Hence, estimating floe size distributions contributes to the understanding of the behavior of the sea-ice extent on a global scale. In addition to this, the floe size distribution is also important in ice management for Arctic offshore operations [4], [5], for example:

1. The efficiency of ice management for Arctic offshore operations and automatically detect hazardous conditions, for example, by identifying large floes that escape the icebreakers operating upstream of a protected structure. The size and shape of managed floes can be identified by the image processing system, compared with limit values, and further processed by the risk management system.
2. Estimate the ice loads on stationary Arctic offshore structures by empirical formulas [6], [7].
3. Initialize high-fidelity numerical models [8]–[13] and validate these at various moments in time by matching the simulated ice fields with the actual ones. Provide an early warning of an ice compaction event, which can be dangerous if the ice-structure interaction

mode changes from a “slurry flow” type to a “pressured ice” type [7], [14].

Automatic identification of individual floe edges is a key tool for extracting information of floe size distribution from aerial images. In an actual ice-covered environment, ice floes typically touch each other, and the junctions may be difficult to identify in digital images. This issue challenges the boundary detection of individual ice floes and significantly affects ice floe size analysis. Several researchers have tried to mitigate this issue. In [19] and [20], the authors separated closely distributed ice floes by setting a threshold higher than the ice-water segmentation threshold and separated the connected ice floes manually when the threshold did not work well. In [17] and [21], the authors applied and compared derivative and morphology boundary detection algorithms in both model ice and sea-ice images. However, non-closed boundaries are often produced by traditional derivative boundary detection, while some boundary information is often lost by morphology boundary detection.

To separate connected sea-ice floes into individual floes, the watershed transform (widely used in connected object segmentation) was adopted in [22] and [23]. Due to an ineluctable over-segmentation problem of the watershed-based method, the authors in [22] manually removed these over-segmented lines, while those in [23] automatically removed the over-segmented lines whose endpoints were both convex. However, over- and under segmentation still affected the ice floe detection results. In [24] and [25], the authors introduced a mathematical morphology together with principal curve clustering to identify ice floes and their boundaries in an almost fully automated manner. Their method operated on the binary images and focused on the morphological characteristics of ice floes rather than on the real boundaries. It was limited by crowded ice floe images, in which the ice floes in the mass were connected to each other, and no “hole” or concave regions could be found after binarization. Those methods are not applicable in our research because of these limitations.

To separate seemingly connected floes into individual ones, a gradient vector flow (GVF) snake algorithm [26] is applied in this research. However, to start the algorithm, a proper initial contour is required for the GVF snake to evolve correctly. Therefore, a manual initialization is typically needed, particularly in crowded floe segmentation. To solve this problem, an automatic contour initialization is proposed to avoid manual interaction and reduce the time required to run the algorithm. Once individual ice floes have been identified, the floe boundaries are obtained, and the floe size distribution can be calculated from the resulting data.

## II. ICE IMAGE PROCESSING METHODS

### A. Ice Pixel Extraction :

Due to the fact that sea ice is whiter than open water, the pixel values differ under normal conditions. See Fig. 2, for example, ice pixels have higher intensity values than those belonging to water in a uniform illumination ice image. Therefore, ice pixels can be extracted by using the thresholding method [27]. Most of the ice can then be identified, as shown in Fig. 3 based on Fig. 2. Of the ice pixels identified, however, only “light ice” has larger pixel intensity values than the threshold. “Dark ice,” with pixel intensity values between the threshold and water, such as ice pieces under the water surface, may not be identified and thus considered to be water, according to the thresholding method



**Fig1: Original sea-ice image.**

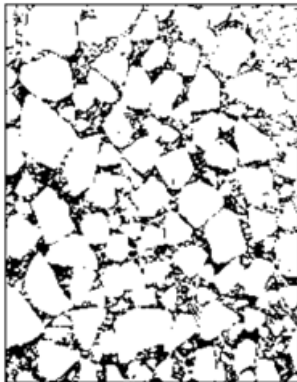


**Fig2: Ice extraction using the *k*-means method.**

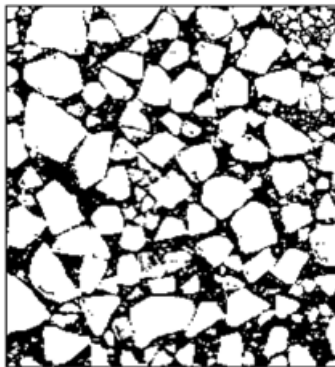


**Fig 3: "Light ice" extracted by the thresholding method.**

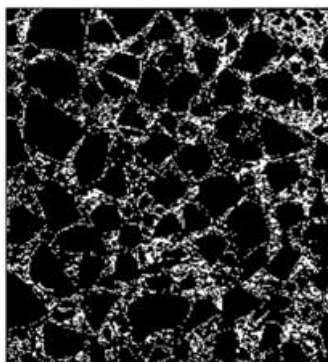


**Fig4: "Dark ice" found by subtracting**

Both "light ice" and "dark ice" pixels are required for an accurate analysis. To distinguish "dark ice" from open water, the *k*-means clustering algorithm [28] can be applied. This minimizes the within-cluster summed distance to partition a set of data into *k* clusters. The image is then divided into three or more clusters, using the *k*-means algorithm.

The cluster with the lowest average intensity value is considered to be water, while the other clusters are considered ice, as shown in Fig. 3. The "dark ice" is then obtained by comparing the difference between Figs. 2 and 3, as shown in Fig. 4.

### **B. Ice Edge Detection:**

The most challenging task is to identify individual ice floes in the sea-ice image, in particular separating the floes that are very close or connected to each other. The boundaries between apparently connected floes have a similar brightness to the floes themselves. The boundaries are too weak to be detected directly, which significantly affects the ice floe statistical result. Therefore, the GVF snake algorithm is proposed to solve this problem. The GVF snake algorithm [26] is able to detect the weak connections between floes and ensure that the detected boundary is closed. As an example, shown in Fig. 6(b), given an initial contour (red curve), the snake finds the floe boundary (green curve) after a few iterations (yellow curves). The GVF snake algorithm relaxes the requirements of the initial contour. However, a proper initial contour for an object is still necessary, particularly to identify the mass of ice floes in an ice image.

Many initial contours are required when performing the GVF snake algorithm to identify all individual ice floes, and these should have proper locations and shapes. An automatic contour installation algorithm is therefore devised to increase the efficiency of the ice floe segmentation method based on the GVF snake algorithm. The GVF snake algorithm [26] is able to detect the weak connections between floes and ensure that the detected boundary is closed. As an example, shown in Fig. 6(b), given an initial contour (red curve), the snake finds the floe boundary (green curve) after a few iterations (yellow curves). The GVF snake algorithm relaxes the requirements of the initial contour. However, a proper initial contour for an object is still necessary, particularly to identify the mass of ice floes in an ice image. Many initial contours are required when performing the GVF snake algorithm to identify all individual ice floes, and these

should have proper locations and shapes. An automatic contour installation algorithm is therefore devised to increase the efficiency of the ice floe segmentation method based on the GVF snake algorithm. Fig. 6 illustrates the floe boundary detection results affected by initializing the contour at different locations. In Fig. 6(a), the initial contour is located at the water, close to the ice boundaries. The snake rapidly detects the boundaries, however, not the ice but the boundaries of the water region. When initializing the contour at the center of an ice floe, as shown in Fig. 6(b), the snake accurately finds the boundary after a few iterations. A weak connection will also be detected if the initial contour is located on it, as shown in Fig. 6(c).

However, when the initial contour is located near the floe boundary inside the floe, as shown in Fig. 6(d), the snake may only find a part of the floe boundary near the initial contour. It should be noted that the curve is always closed, regardless of how it deforms, even in the cases of Fig. 6(c) and (d), which appear to be non-closed curves. This behavior occurs because the area bounded by the closed curve tends toward zero. For example, Fig. 8(a) shows a small binary image matrix for a simple shape, and the matrix in Fig. 8(b) shows the corresponding distance transform (using “City Block” distance metrics). The local maximum is the pixel whose value is greater or equal to any of its neighbors, as shown by the green numerals in Fig. 8(b).

A local maximum of the distance transform ideally corresponds to the center of an object, but more than one local maximum are detected in many cases. Thus, a dilation operator [31] is used to merge the local maxima within a short distance (within a threshold  $T$ ) of each other. The centers of the dilated regions [red “+” in Figs 8(b) and 9(b)], which are called “seeds,” is chosen as the locations of our initial contours.

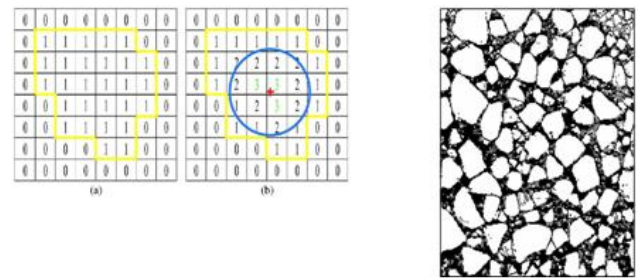
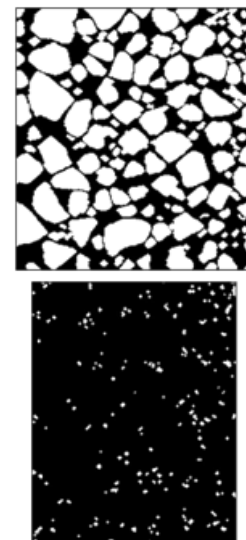


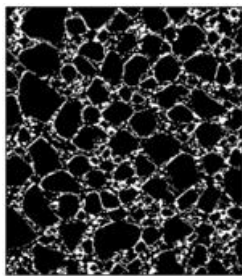
Fig: Layer showing the “brash ice” in Fig. 1

C. Fig: Ice Shape Enhancement:

Because of the noise, some floes may contain holes or smaller ice pieces inside. For example, Fig. 11(a), which is extracted from Fig. 2, shows an ice floe with speckle. Because of the uneven grayscale of the ice floe, the lighter part of the floe is considered as “light ice” [the white pixels in Fig. 11(b) and (c)], whereas the darker part is considered as “dark ice” [the gray pixels in Fig. 11(b) and (c)] by the  $k$ -means and threshold method. This means that the ice floe cannot be completely identified, and the shape of the detected ice floe is rough, as shown in Fig. 11(b).will ensure the completeness of the ice floe, and smaller ice floes or brash pieces contained in a larger ice floe are removed.



Contour initialization algorithm. (a) Binary image matrix. (b) Distance transform of (a), local maximum, seed, and initial contour.



**D. Ice Type Classification and Floe Size Distribution:**

According to [33], brash ice is considered as floating ice fragments no more than 2 m across. To distinguish brash ice from ice floes in our algorithm, we define a brash-ice threshold parameter (pixel number or area) that can be tuned for each application. The ice pieces with size larger than the threshold are considered to be ice floes, while smaller pieces are considered to be brash ice. The remaining ice pixels in Fig. 4 were labeled as slush. The result is four layers of a sea-ice image (using Fig. 2 as an example): ice floe (see Fig. 13), brash ice (see Fig. 14), slush (see Fig. 15), and water (see Fig. 16).

Based on the four layers, a total of 154 ice floes and 189 brash ice pieces are identified in Fig. 2. The coverage percentages are 60.52% ice floe, 3.34% brash ice, 16.03% slush, and 20.11% water. The ice floe (brash) size can be determined by the number of pixels in the identified floe (brash). If the focal length  $f$  and camera height are available, the actual size in SI unit of the ice floes and floe size distribution can be also calculated [34] by converting the image pixel size to its SI unit size. The ice floe size (calculated by counting the pixel number of the floe) distribution histogram is shown in Fig. 17. The residue ice, which is the detected boundary pixels between the connected floes, was previously considered as slush.

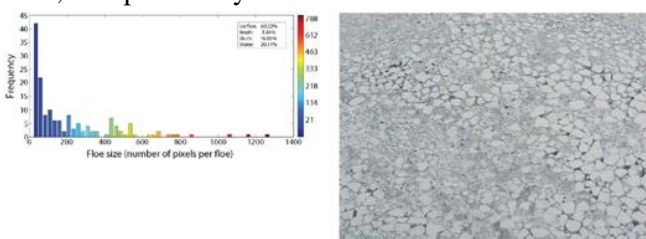


Fig. .Floe size distribution histogram of Fig. 13.

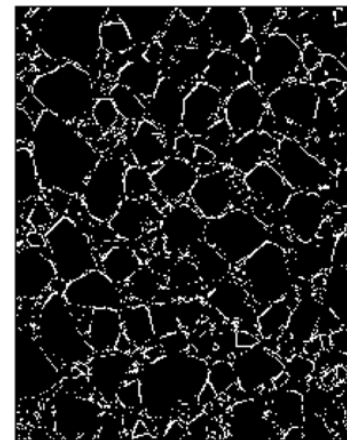


Fig. .Sea-ice image.

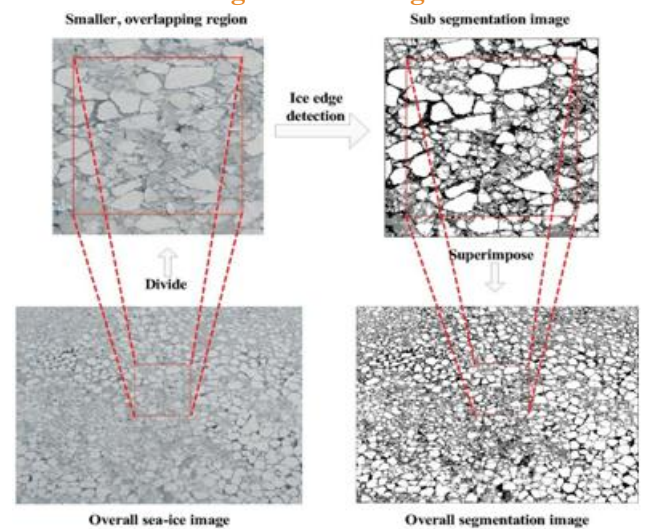


Fig.. Residue ice (boundary pixels).

**C. Results:**

After orthorectification, we enhance the shapes of all the ice pieces (Algorithm 2), and finally, we obtain the ice floe and brash ice size distribution, as shown in Fig. 22. Brash ice is dark blue, smaller floes are light blue, and larger floes are red. Brash positions are not shown, whereas the floe positions are denoted using a black dot. A total of 2511 ice floes and 2624 brash ice are identified in Fig. 19. The coverage percentages are 65.98% ice floe, 5.03% brash ice, 17.52% slush, and 11.47% water. Instead of the actual size of ice floe and brash (since we do not have the height above sea level for the camera), the ice floe (brash) size is calculated by the number of pixels in the identified floe (brash).

The relative ice floe distribution histogram is derived and shown in Fig. 23, and the overall algorithm of the case study is concluded in Algorithm 3.

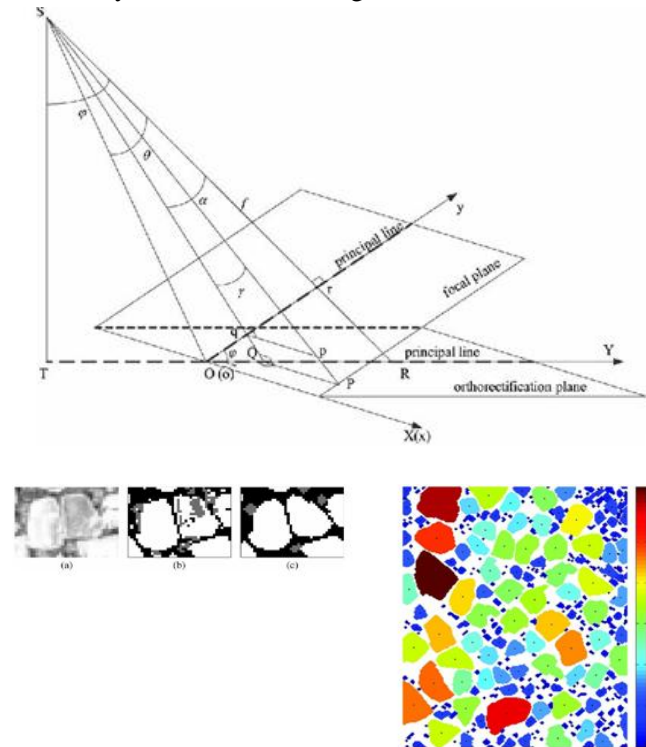


Fig: Sea Ice floes Detection

#### IV. CONCLUSION:

A remote sensing mission yielded experience in data acquisition using a UAV. Various image processing methods were applied to a few samples of the collected sea-ice image data for analysis to retrieve important sea-ice information. Focusing on identifying the non-ridged ice floe in the marginal ice zone, and the managed ice resulting from offshore operations in sea ice, we proposed an algorithm to identify the individual ice floes in a sea-ice image using the GVF snake algorithm.

To evolve the GVF snake automatically, “light ice” and “dark ice” were first obtained using the thresholding and *k*-means algorithms. The initial contours of both “light ice” and “dark ice” with proper locations and radii were then derived based on the local maxima from the distance transform. After ice edge detection, morphological cleaning was used to enhance floe shapes.

The implementation on the sea-ice images, which contained multiple ice floes crowded together, is shown to give acceptable segmentation results.

#### REFERENCES:

- [1] S. Løset, K. N. Shkhinek, O. T. Gudmestad, and K. V. Hyland, *Actions from Ice on Arctic Offshore and Coastal Structures*. St. Petersburg, Russia: Lan Publishing House, 2006.
- [2] W. Peter, *Ice in the Ocean*. New York, NY, USA: Taylor & Francis, 2000.
- [3] T. Toyota and H. Enomoto, “Analysis of sea ice floes in the sea of Okhotsk using ADEOS/AVNIR images,” in *Proc. 16th IAHR Int. Symp. Ice*, Dunedin, New Zealand, 2002, pp. 211–217.
- [4] A. Keinonen, “Ice management for ice offshore operations,” in *Proc. Offshore Technol. Conf.*, Houston, TX, USA, 2008, pp. 690–704.
- [5] J. Hamilton et al., “Ice management for support of arctic floating operations,” in *Proc. OTC Arctic Technol. Conf.*, Houston, TX, USA, 2011, pp. 615–626.
- [6] A. Keinonen and I. Robbins, “Icebreaker characteristics synthesis, icebreaker performance models, seakeeping, icebreaker escort,” in *Icebreaker Escort Model User’s Guide: Report Prepared for Transport Development Centre Canada (TP12812E)*, vol. 3. Calgary, AB, Canada: AKAC, 1998, p. 49.
- [7] A. Palmer and K. Croasdale, *Arctic Offshore Engineering*. Singapore: World Scientific, 2012.
- [8] C. Daley, S. Alawneh, D. Peters, B. Quinton, and B. Colbourne, “GPU modeling of ship operations in pack ice,” in *Proc. Int. Conf. ICETECH Exhib. Perform. Ships Struct.*, Banff, AB, Canada, 2012, pp. 122–127.
- [9] G. Vachon, M. Sayed, and I. Kubat, “Methodology for determination office management efficiency,” in *Proc. Int. Conf. ICETECH Exhib. Perform. Ships Struct.*, Banff, AB, Canada, 2012, pp. 346–353.
- [10] M. Sayed et al., “Numerical simulations of ice interaction with a moored structure,” in *Proc. Int. Conf.*

ICETECH Exhib. Perform. Ships Struct., Banff, AB, Canada, 2012, pp. 159–166.

[11] M. Sayed, I. K. Kubat, and B. Wright, “Numerical simulations of ice forces on the Kulluk: The role of ice confinement, ice pressure and ice management,” in Proc. OTC Arctic Technol. Conf., Houston, TX, USA, 2012, pp. 965–973.

[12] A. Gürtner, B. Bjørnsen, T. H. Amdahl, S. R. Sberg, and S. H. Teigen, “Numerical simulations of managed ice loads on a moored Arctic drillship,” in Proc. OTC Arctic Technol. Conf., Houston, TX, USA, 2012, pp. 914–920.

[13] I. Metrikin, S. Løset, N. A. Jenssen, and S. Kerkeni, “Numerical simulation of dynamic positioning in ice,” *Marine Technol. Soc. J.*, vol. 47, no. 2, pp. 14–30, Mar./Apr. 2013.

[14] B. Wright et al., “Evaluation of full scale data for moored vessel station keeping in pack ice,” B. Wright & Associates Ltd., Canmore, AB, Canada, PERD/CHC Report 26-200, 1999.

[15] J. Haugen, L. Imsland, S. Løset, and R. Skjetne, “Ice observer system for ice management operations,” in Proc. 21st Int. Ocean Polar Eng. Conf., Maui, HI, USA, 2011, p. 1120. [16] P. Lu, Z. Li, Z. Zhang, and X. Dong, “Aerial observations of floe size distribution in the marginal ice zone of summer Prydz Bay,” *J. Geophys. Res., Oceans*, vol. 113, no. C2, pp. C02011-1–C02011-11, Feb. 2008.

[17] Q. Zhang, R. Skjetne, S. Løset, and A. Marchenko, “Digital image processing for sea ice observation in support to Arctic DP operation,” presented at the Proc. 31st International Conf. Ocean, Offshore Arctic Engineering, Rio de Janeiro, Brazil, 2012, Paper OMAE2012-83860.

[18] M. Eldridge et al., “Design and build a search and rescue UAV,” Univ. Adelaide, Adelaide, Australia, 2009.

[19] T. Toyota, S. Takatsuji, and M. Nakayama, “Characteristics of sea ice floe size distribution in the seasonal ice zone,” *Geophys. Res. Lett.*, vol. 33, no. 2, pp. L02616-1–L02616-4, Jan. 2006.

[20] T. Toyota, C. Haas, and T. Tamura, “Size distribution and shape properties of relatively small

sea-ice floes in the Antarctic marginal ice zone in late winter,” *Deep Sea Res. II, Top. Studies Oceanogr.*, vol. 58, no. 9/10, pp. 1182–1193, May 2011.

[21] Q. Zhang, S. van der Werff, I. Metrikin, S. Løset, and R. Skjetne, “Image processing for the analysis of an evolving broken-ice field in model testing,” presented at the 31st Int. Conf. Ocean, Offshore Arctic Engineering, Rio de Janeiro, Brazil, 2012, Paper OMAE2012-84117.

[22] J. Blunt, V. Garas, D. Matskevitch, J. Hamilton, and K. Kumaran, “Image analysis techniques for high Arctic, deepwater operation support,” in Proc. OTC Arctic Technol. Conf., Houston, TX, USA, 2012, pp. 986–996.

[23] Q. Zhang, R. Skjetne, and B. Su, “Automatic image segmentation for boundary detection of apparently connected sea-ice floes,” in Proc. 22<sup>nd</sup> Int. Conf. Port Ocean Eng. Arctic Conditions, Espoo, Finland, 2013, pp. 303–310. [24] J. Banfield, “Automated tracking of ice floes: A stochastic approach,” *IEEE Trans. Geosci. Remote Sens.*, vol. 29, no. 6, pp. 905–911, Nov. 1991.

[25] J. D. Banfield and A. E. Raftery, “Ice floe identification in satellite images using mathematical morphology and clustering about principal curves,” *J. Amer. Stat. Assoc.*, vol. 87, no. 417, pp. 7–16, Mar. 1992.

[26] C. Xu and J. L. Prince, “Snakes, shapes, and gradient vector flow,” *IEEE Trans. Image Process.*, vol. 7, no. 3, pp. 359–369, Mar. 1998.

[27] N. Otsu, “A threshold selection method from gray-level histograms,” *Automatica*, vol. 11, no. 285–296, pp. 23–27, 1975.

[28] J. MacQueen et al., “Some methods for classification and analysis of multivariate observations,” in Proc. 5th Berkeley Symp. Math. Stat. Probab., Berkeley, CA, USA, 1967, vol. 1, pp. 281–297.

[29] M. Kass, A. Witkin, and D. Terzopoulos, “Snakes: Active contour models,” *Int. J. Comput. Vis.*, vol. 1, no. 4, pp. 321–331, Jan. 1988. [30] A. Rosenfeld and J. L. Pfaltz, “Distance functions on digital pictures,” *Pattern Recognit.*, vol. 1, no. 1, pp. 33–61, Jul. 1968.

[31] R. C. Gonzalez, R. E. Woods, and S. L. Eddins, *Digital Image Processing Using MATLAB*. Upper Saddle River, NJ, USA: Prentice-Hall, 2003.

[32] L.-K. Soh, C. Tsatsoulis, and B. Holt, "Identifying ice floes and computing ice floe distributions in SAR images," in *Analysis of SAR Data of the Polar Oceans*. Berlin, Germany: Springer-Verlag, 1998, pp. 9–34.

[33] WMO SEA-ICE NOMENCLATURE, (accessed 2014-08-31). [Online]. Available: <http://www.aari.ru/gdsidb/XML/volume1.php?lang1=0&arrange=>

[34] P. Lu and Z. Li, "A method of obtaining ice concentration and floe size from shipboard oblique sea ice images," *IEEE Trans. Geosci. Remote Sens.*, vol. 48, no. 7, pp. 2771–2780, Jul. 2010.

[35] T. Lippmann and R. A. Holman, "Quantification of sand bar morphology: A video technique based on wave dissipation," *J. Geophys. Res., Oceans*, vol. 94, no. C1, pp. 995–1011, Jan. 1989. P. Smith, "Bilinear interpolation of digital images," *Ultramicroscopy*, vol. 201–204, 1981.